

Towards Natural Language-Guided Drones: GeoText-1652 Benchmark with Spatially Relation Matching

Meng Chu, Zhedong Zheng, Wei Ji, Tat-Seng Chua
National University of Singapore

Abstract

Drone navigation through natural language commands remains a significant challenge due to the lack of publicly available multi-modal datasets and the intricate demands of fine-grained visual-text alignment. In response to this pressing need, we present a new human-computer interaction annotation benchmark called *GeoText-1652*, meticulously curated through a robust Large Language Model (LLM)-based data generation framework and the expertise of pre-trained vision models. This new dataset seamlessly extends the existing image dataset, i.e., *University-1652*, with spatial-aware text annotations, encompassing intricate image-text-bounding box associations. Besides, we introduce a new optimization objective to leverage fine-grained spatial associations, called *blending spatial matching*, for region-level spatial relation matching. Extensive experiments reveal that our approach maintains an exceptional recall rate under varying description complexities. This underscores the promising potential of our approach in elevating drone control and navigation through the seamless integration of natural language commands in real-world scenarios.

1. Introduction

Drone navigation using natural language offers potential to a range of applications such as disaster management [27, 30], live search and rescue [3, 26], and remote sensing [2, 4, 13, 14]. Given one single input image, drone navigation is to search the other relevant images of the same place from a large-scale gallery [32, 35, 36, 45, 48, 49], which is usually regarded as a sub-task of image retrieval. Current datasets typically provide pairs of images, focusing on matching images from disparate platforms like drones and satellites [15, 17, 29, 47, 52]. However, the query image is not always available, while natural language description is a more intrinsic input modality from the user. There remains two challenge towards natural language-guided drone navigation: (1) There is no large public language-guided dataset. Providing such a detailed description of the image is usually challenging with high human resource costs

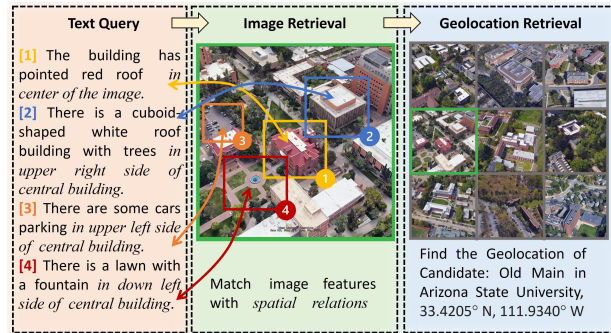


Figure 1. An example of the proposed benchmark, **GeoText-1652**. Here we show a text-guided drone navigation process. Left: Every image contains several region-level query sentences. Middle: Given the user description, we match the text and region of interest with the spatial relation. Right: With the dense spatial relation matching, we could easily retrieve the place of interest against other similar false-positives, and navigate the drone.

and reliable annotation quality. (2) It remains challenging to align language and visual representation, of the fine-grained nature in the drone-view scene images.

For the first limitation, we propose a multi-view, multi-source vision-language dataset *GeoText-1652*, drawing on the existing multi-source images dataset, *University-1652* [49] (see Figure 1). We have established links between locational data and corresponding textual descriptions through a semi-automatic process, annotation including 276,045 text-bbox pairs and 316,335 descriptions. Our benchmark facilitates two new tasks: drone navigation via text and drone-view target localization. As the name implies, drone navigation via text focuses on the strategic guidance of a drone to the location it has previously visited that most closely aligns with a provided textual description. This involves a fine-grained text-to-image retrieval process, highlighting the integration between linguistic and spatial data. On the other hand, drone-view target localization focuses on identifying the textual description that best matches a drone-captured image to accurately localize a target, which is an image-to-text retrieval task. In our experimental setup, we approach these tasks as challenges in cross-modal retrieval focusing on bridging different types

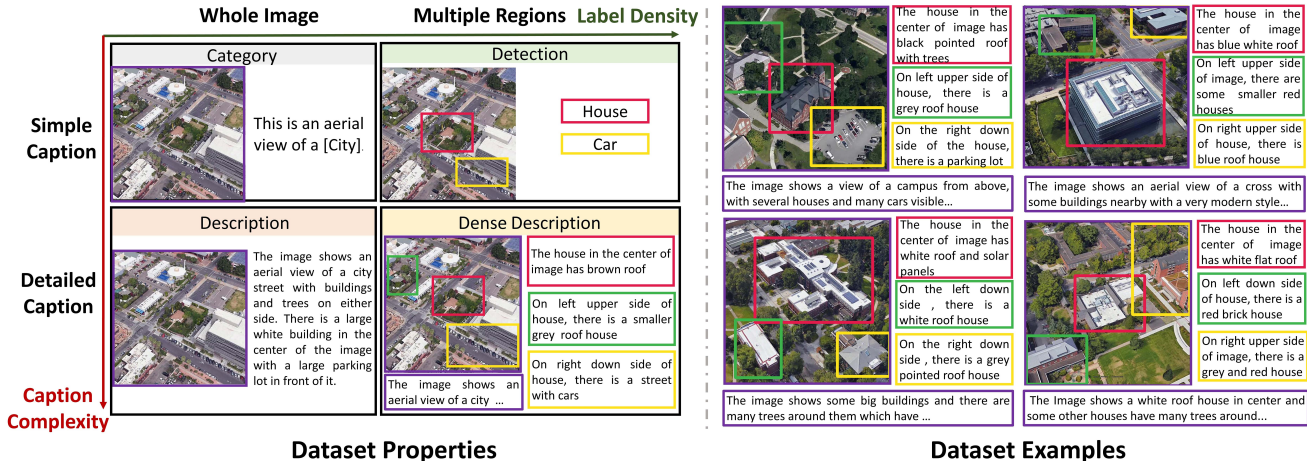


Figure 2. **The properties of the proposed dataset GeoText-1652.** Different from the traditional category annotation, our dataset not only includes image-level detailed descriptions but region-level short descriptions (left). Samples of the dataset show that the description could align well with the image and its regions (right).

of data representations. We compare the generic feature trained on extremely large datasets with the viewpoint-invariant feature learned on our proposed dataset. We observe that the proposed GeoText-1652 dataset aids in learning the viewpoint-invariant feature, which refines drone control via language, making it more precise and intuitive. To address the second challenge, we introduce an approach for spatial relation matching that leverages the GeoText-1652 dataset. Our methodology encompasses two losses, grounding loss and spatial loss, which help the model in understanding the spatial relationships between objects within images. Through this approach, we enhance the capability of the model in deciphering spatial correlations, paving the way for more precise text-to-image retrieval. The key contributions of our work are as follows:

- In pursuit of facilitating natural language-guided drone control, we introduce a new image-text-bbox benchmark, called GeoText-1652, which expands on the existing multi-platform image dataset. In particular, we focus on establishing a connection between position and text annotation using human-computer interaction annotation.
- As a minor contribution, we introduce a new spatial-aware approach, that explores the region-level relationship between drone images and text. In contrast to conventional image-text mutual search methodologies, our approach capitalizes on positional relationships within drone images and textual descriptions of surrounding positions to achieve more precise localization.
- Our proposed spatial-aware model has achieved 32.3% recall@10 accuracy using text query, surpassing established models, such as, ALBEF [17], and X-VLM [46]. We also observe that the learned model could generalize to real-world scenarios.

2. Related Works

Cross-view Geo-localization. Cross-view geo-localization addresses the challenge of associating images captured from different viewpoints with their corresponding geographical locations [1, 16, 37, 39, 49]. One key underpinning this task is to extract a discriminative visual representation against viewpoints. For instance, Wang *et al.* [40] develop a partitioning strategy that enriches the feature set by considering multiple parts of the image and Lin *et al.* [21] introduce a new attention module to discover representative key points and focus on the salient region. Dai *et al.* [7] introduce a transformer-based structure with a content alignment strategy. Similarly, Yang *et al.* [43] utilize the properties of self-attention and exploit the positional encoding of ground and aerial images. Rodrigues *et al.* [33] introduce a dual path network to fuse the local region with the global feature for partial aerial-view image matching. Another line of works [5, 9, 12, 34, 48, 54] further integrate enhanced features across different model designs and leverage extra knowledge to improve geo-localization. Shi *et al.* [34] fuse the pose estimation and geometry projection into the feature matching, while Hu *et al.* [12] emphasize the accuracy of orientation in street-view images. Chen *et al.* [5] introduce a cross-drone mapping mechanism in the transformer. GeoDTR [48] employs two data augmentation techniques to capture both low-level details and spatial configurations. TransGeo [54] combines transformer flexibility and attention-guided non-uniform cropping to enhance image resolution in key areas. Dhakal *et al.* [9] design one contrastive learning framework, which could predict textual embedding for ground-level scenery. Different from existing methods, our work focuses on two new natural language-guided drone tasks, which provide a straight-

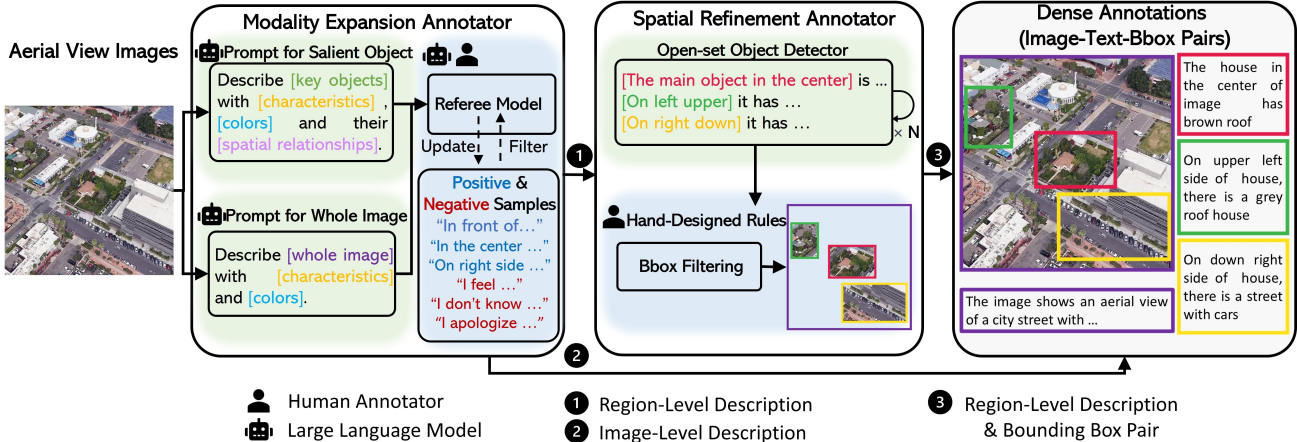


Figure 3. **The proposed human-computer interaction annotation strategy.** The strategy includes two main processes: modality expansion annotator and spatial refinement annotator. The modality expansion annotator is to annotate the image-level and the region-level descriptions. The spatial refinement annotator could utilize the region-level description to conduct the visual grounding. Finally, after some filtering processes, we build the proposed dataset with Image-Text-Bbox Pairs.

forward way to control the drone.

Multi-modality Alignment. In this work, we focus on natural language-guided navigation, which can be viewed as a sub-task of text-to-image retrieval [6, 11, 15, 17, 18, 20, 29, 46]. Early works usually focus on structure design, such as dual-path network [50]. Wang *et al.* [41] employ an adaptive gating scheme to handle negative pairs and irrelevant information, calculating the matching score based on the fused features, while Li *et al.* [19] apply graph convolutional networks for semantic reasoning within image regions. Then, Chen *et al.* [6] propose word region alignment in the pertaining of multimodal model with large-scale datasets. Li *et al.* [20] apply object tags detected in images as anchor points to ease the learning of alignments, while Yang *et al.* [44] study the attribute-related keywords. Clip model [29] proposes a contrastive learning method between image-text pairs. Jia *et al.* [15] design a simple dual-encoder architecture to align visual and language representations. Li *et al.* [17] refine image text matching loss with a self-training method which learns from pseudo-targets. Zeng *et al.* [46] further align multi-region visual concepts and associated texts. Blip model [18] leverages noisy web data through a caption bootstrapping process. Different from these existing works, we introduce a new spatial-aware approach, which explicitly considers fine-grained spatial text-region matching. For instance, when similar elements appear within a single image, the model may incorrectly align them if it fails to discern the nuances in their spatial relations.

Split	#imgs	#global deps	#Bbox-Texts	#classes	#unis
Training _{drone}	37,854	113,562	113,367	701	
Training _{satellite}	701	2,103	1,709	701	33
Training _{ground}	11,663	34,989	14,761	701	
Test _{drone}	51,355	154,065	140,179	951	
Test _{satellite}	951	2,853	2,006	951	39
Test _{ground}	2,921	8,763	4,023	793	

Table 1. **Statistics of GeoText-1652.** Training and test sets all include the image, global description, bounding box and building numbers. The test set only uses the image and global description during the test process. We note that there is no overlap between the 33 universities of the training set and the 39 universities of the test sets. Three platforms are considered, *i.e.*, drone, satellite, and ground cameras.

3. GeoText-1652 Dataset

3.1. Dataset Description

The proposed GeoText-1652 dataset extends the image-based University-1652 dataset, containing 1,652 buildings from 72 universities. The images are collected from three platforms, *i.e.*, satellite-view, drone-view and ground-view images. All images are annotated with 3 global descriptions and 2.62 bounding boxes on average since we removed some low-quality bounding boxes. On average, each global description, encompassing both image-level and region-level details, contains 70.23 words. As shown in Figure 2, the proposed dataset, compared to the original dataset, contains fine-grained descriptions with region-level annotations, which is key to the natural language-guided task. The region-level descriptions, extracted specifically for bounding box matches, contain 21.6 words on average. More detailed statistics are shown in Table 1.

3.2. Dataset Annotation Framework

As shown in Figure 3, we briefly illustrate the overall workflow of our dataset construction for the navigation via nature language task. We extend the conventional drone-view dataset University-1652 with dense annotations. To generate image-text pairs for the University-1652 dataset, we adopt a new human-computer interaction annotation strategy, which could largely save time and costs. The annotation process can be delineated into two principal phases, *i.e.*, the modality expansion phase and the spatial refinement phase. **(1)** For the modality expansion phase, we apply two kinds of prompts for each image. One prompt focuses on salient objects and the other prompt encompasses the description of the entire image. Given the input and prompts, we ask the visual language model (visual-LLM [51]) to answer. Given the inherent limitations of language models, not all answer meets the standards, such as hallucination phenomena and ambiguous statement. To address this limitation, we introduce a referee model to autonomously adjudicate whether the outputs from visual-LLM meet good quality. In particular, the raw annotations first undergo positive sample element detection to ensure the inclusion of the desired keywords, then enter a negative sample pool to exclude subjective statements. The keyword within the referee model is set by the human-computer interaction. In particular, given several raw answers, we adopt a large language model [28] as a teacher to classify the negative and positive samples. Considering the high cost of annotating all answers, we involve the human annotator to check these positive or negative samples and designs some simple keyword filtering rule to remove the common faults. In this way, we could obtain 3 image-level descriptions and 9 region-level description proposals for every input image. **(2)** Taking one step further, we intend to build the relation with the bounding box in the spatial refinement phase. Specifically, given the region-level description, we utilize one off-the-shelf text-based visual grounding model [23] to identify corresponding bounding boxes (Bboxes). Since all region-level description contains spatial phrases such as ‘right’ or ‘left’, we set a spatial rule to filter out the bounding boxes with the wrong places. We also, in turn, refine the description by adding vertical words, such as ‘upper left’, and ‘down right’. Therefore, given 9 region-level description proposals, we only annotate 2.62 corresponding bounding boxes on average. Finally, through the stages of modality expansion and spatial refinement annotator, we achieve a dense annotation, encompassing both image-level descriptions and region-level descriptions with Bbox pairings.

Discussion. The contribution to the community. The key difference from existing datasets [22, 42, 53] lies in the fine-grained region-level descriptions, facilitating more nuanced natural language-guided tasks (see Table 2). This level of detail is crucial for tasks requiring precise localiza-

Property	CVUSA[42]	CVACT[22]	VIGOR[53]	GeoText-1652
Annotation	GPS Tag	GPS Tag	GPS Tag	Sentence
# Bbox-Texts	N/A	N/A	N/A	276,045
Platform	G,S	G,S	G,S	G,S,D
Modality	Image	Image	Image	Image, Text

Table 2. **Dataset Comparison.** Comparison between the proposed Geo-Text-1652 and other existing geo-localization datasets. G, S, and D denote ground-view, satellite-view and drone-view image, respectively.

tion and contextual understanding. Moreover, our dataset annotation framework, incorporating a human-computer interaction strategy and a referee model, ensures both efficiency and high-quality annotations. Researchers can leverage GeoText-1652 to explore new approaches, improve model generalization, and push the boundaries of visual geo-localization and natural language understanding integration.

4. Method

As shown in Figure 4, we introduce a cross-modal geo-localization framework to conduct intricate spatial analyses, merging visual and textual data. It consists of an image encoder, a text encoder, and a cross-modal encoder. All encoders are based on transformer [38]. Except for the traditional Image-text Semantic Matching in Section 4.1, we introduce a new blending spatial matching in Section 4.2.

4.1. Image-text Semantic Matching

Image-Text Contrastive. Given an image-text pair, we first extract the image visual feature V and image-level text feature T , respectively. Cosine similarity can be calculated as: $s(V, T) = \frac{V^T T}{\|V\|_2 \|T\|_2}$. According to contrastive learning, we treat the other samples within the mini-batch as negative examples. Then, we could calculate the in-batch vision-to-text and text-to-vision similarity as:

$$p_{v2t} = \frac{\exp(s(V, T)/\tau)}{\sum_{i=1}^N \exp(s(V, T^i)/\tau)}, \quad (1)$$

$$p_{t2v} = \frac{\exp(s(V, T)/\tau)}{\sum_{i=1}^N \exp(s(V^i, T)/\tau)}, \quad (2)$$

where τ is a learnable temperature parameter. The superscript of V and T denotes the i -th sample within the batch. The contrastive learning is defined as the cross-entropy loss:

$$\mathcal{L}_{itc} = -\frac{1}{2} \mathbb{E} [\log(p_{t2v}) + \log(p_{v2t})], \quad (3)$$

where we encourage that the identity image-text pair has the larger similarity.

Image-Text Matching. We further demand the model to determine whether a pair of visual concepts and text is

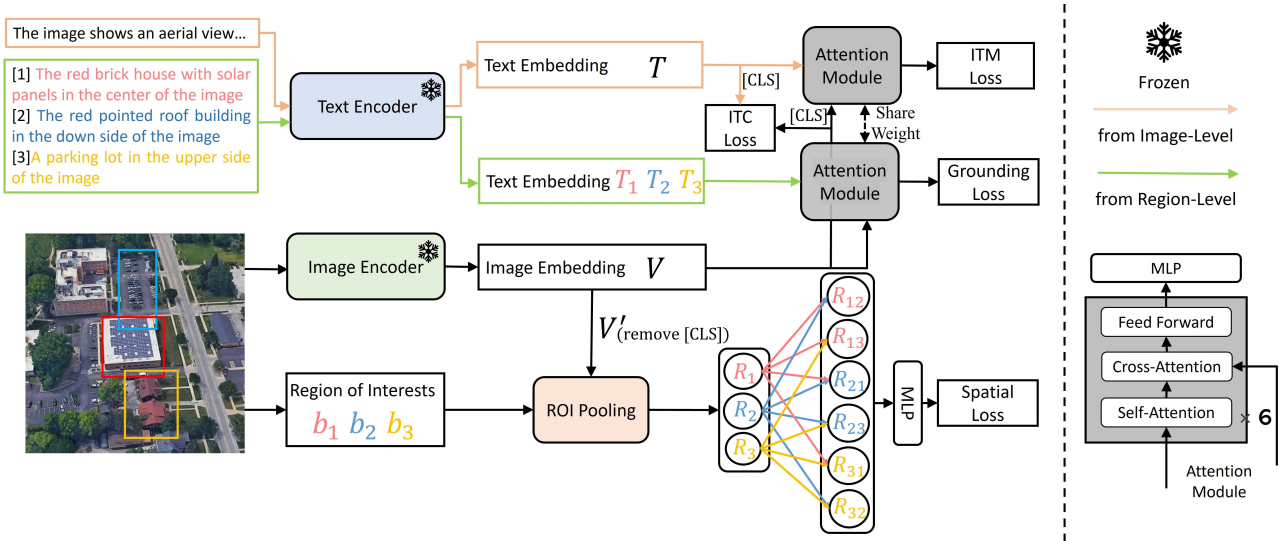


Figure 4. **The proposed multi-modal framework.** The framework processes an aerial image by identifying regions of interest (ROIs) and matching them with corresponding text descriptions. It contains an image encoder that extracts visual embeddings and intermediate feature maps. We could obtain region-level visual features via ROI Pooling, and concatenate to calculate the spatial relation followed by multi-layer perceptron (MLP). On the other hand, text inputs, including the image-level and region-level descriptions, are encoded separately with the text encoder. Two attention modules integrate the image and text features, and they share the same weights. The framework applies several loss functions, including Grounding and Spatial Loss for blending spatial matching, and ITM and ITC Loss for image-text matching.

matched. For each visual concept in a mini-batch, we sample an in-batch hard negative text feature according to the highest similarity in Equation 2. Similarly, we also sample one hard negative visual feature for each text. We use the output embedding of the cross-modal encoder to predict the matching probability p_{match} , and the binary classification loss is:

$$\mathcal{L}_{\text{itm}} = -\mathbb{E}[\mathbf{y} \log(p_{\text{match}}) + (1 - \mathbf{y}) \log(1 - p_{\text{match}})], \quad (4)$$

where \mathbf{y} is a binary label indicating whether the input is a positive pair or a hard negative pair.

4.2. Blending Spatial Matching

In text-guided bounding-box prediction, known as the grounding process, the model uses natural language descriptions to identify and spatially locate objects within an image. This involves an interaction between the text and image feature maps to guide a region proposal network. Therefore, our proposed blending spatial matching includes two optimization objectives: the grounding prediction and the spatial relation matching.

Grounding Prediction. Given the image representation and the region-level text representation, the model is to predict the bounding box b_j according to the corresponding textual concept T_j . The bounding box is formulated as $b_j = (c_x, c_y, w, h)$. Here the subscript j denotes the j -th short bounding box of the corresponding image. c_x, c_y are the center point coordinate of the bounding box, and h, w are the height and width, respectively. In particular, we

adopt the cross-attention model with six transformer blocks followed by multi-layer perceptron (MLP) (as shown in Figure 4 (right)). We also apply the Sigmoid to normalize the prediction \hat{b}_j within the valid region $[0, 1]$. The grounding prediction loss includes the ℓ_1 regression loss and the Intersection over Union (IoU) loss [31] to compare the overlap areas. Therefore, the grounding loss can be formulated as:

$$\mathcal{L}_{\text{grounding}} = \mathbb{E}[\mathcal{L}_{\text{iou}}(b_j, \hat{b}_j) + \|b_j - \hat{b}_j\|_1]. \quad (5)$$

Spatial Relation Matching. Considering the grounding loss focus on a single region, we propose a relative localization matching. For instance, given the visual feature of three bounding boxes, we intend to predict the spatial relationship between them. Given three regions of interests b_1, b_2, b_3 , we extract the visual feature based on the global feature V via the ROI Pooling module as region features R_1, R_2, R_3 . As the spatial relation is a relative concept, we concatenate the region features as composed feature R_{ij} ($i \neq j$). Then we adopt the Multi-Layer Perceptron (MLP) to predict the 9-class spatial relationship p_r^{ij} . The spatial loss is defined as the cross-entropy loss between \mathbf{y}_r^{ij} and \hat{p}_r^{ij} :

$$\mathcal{L}_{\text{spatial}} = \mathbb{E}[-\mathbf{y}_r^{ij} \log(\hat{p}_r^{ij})], \quad (6)$$

where the ground-truth class \mathbf{y}_r^{ij} is derived by the center distance for the two bboxes (c_x, c_y, w, h) and (c'_x, c'_y, w', h') . Horizontal distance is defined as $\Delta x = c'_x - c_x$ and vertical distance is $\Delta y = c'_y - c_y$. If $|\Delta x| < \frac{w}{2}$,

we define it as ‘middle’; If $\Delta x > \frac{w}{2}$, we define it as ‘left’; If $\Delta x < -\frac{w}{2}$, we define it as ‘right’. Similarly, we also could classify the ground-truth vertical relationship as 3 categories, *i.e.*, top, middle, and bottom. Therefore, we could compose the vertical and horizontal relation as 9 location categories in total.

Discussion. Why do we need spatial relation matching? Relative position estimation has been explored in other fields, such as self-supervised learning [10]. In this work, spatial matching serves as a crucial complement to bounding box prediction in our approach, providing a nuanced perspective on the relationships between different regions of interest (ROIs). While bounding box prediction focuses on individual regions, our proposed relative localization matching introduces a relative spatial dimension to the scene understanding. In particular, the proposed spatial relation matching via 9 orientation classification motivates the model towards a more fine-grained understanding of different regions within the image.

4.3. Optimization Objectives

Finally, the total loss \mathcal{L}_{total} is defined as:

$$\mathcal{L}_{total} = \mathcal{L}_{itc} + \mathcal{L}_{itm} + \lambda(\mathcal{L}_{grounding} + \mathcal{L}_{spatial}), \quad (7)$$

where λ denotes the blending spatial matching weight, and we empirically set $\lambda = 0.1$.

5. Experiment

5.1. Implementation Details

We adopt the XVLM [46] pretrained on 16M images as our backbone model. Our text encoder is BERT [8] and our image encoder is Swin transformer [24]. We deploy AdamW [25] optimizer with a weight decay of 0.01. The learning rate is set to $3e^{-5}$. All the images would be resized to 384×384 pixels during the training process, and the image patch size is set to 32. We perform simple data augmentation techniques, such as brightness adjustment and identity operation. We do not use random rotation or horizontal flipping as it would lose the spatial information. In the context of global description serving as the text query, we remove stop words to keep the query concise during evaluation.

5.2. Geo-localization Results

The GeoText-1652 dataset contributes to the advancement of cross-modality retrieval and the proposed method outperforms the performance of other models, particularly when fine-tuned with this dataset. We could observe two primary points from Table 3:

Effectiveness of the Proposed Dataset. The GeoText-1652 dataset, provides a substantial ground for evaluating the

image-text retrieval capabilities of various models. The results show that fine-tuning our dataset leads to considerable improvements in performance, as seen with ALBEF_{finetuned} and XVLM_{finetuned}, among others. The result also suggests that the dataset contains rich and varied annotations that are beneficial for training models to understand and match images with text descriptions accurately. Furthermore, the significant gap between pre-trained models and their fine-tuned counterparts underscores that it remains challenging for the “large” vision model on the aerial-view dataset, reflecting the necessity of the proposed dataset.

Superiority of the Proposed Method. Our method shows a clear superiority over other methods, particularly in the Recall@10 metric for both image and text retrieval tasks. Compared with the baseline XVLM_{finetuned}, the proposed method moves more positive candidates forward in the ranking list, with +0.5% Recall@1, +2.0% Recall@5 and +2.7% Recall@10 improvements in the text-to-image retrieval. Similarly, we could observe the increase in the image-to-text retrieval setting, with +1.2% Recall@1, +1.2% Recall@5 and +1.3% Recall@10. Such improvement is non-trivial in practical applications, where multiple correct answers are desirable. With comparable model parameters, the high Recall@10 performance also implies that the model is capable of understanding the visual-textual relationship effectively. The proposed approach learns diverse features from the GeoText-1652 dataset, handling the detailed descriptions and region-level annotations efficiently.

5.3. Ablation Study and Further Discussion

Effect of Loss Objectives. We gradually add the loss terms to train the model, and the retrieval performance is shown in Table 4. The baseline model, stripped of both the spatial and grounding loss, exhibits a more significant impairment, as mirrored in the Recall@1 accuracy for Text Query and Image Query. With the grounding loss only, the overall performance of the model is better compared to the baseline model, *i.e.*, +0.3% Recall@1 accuracy in Text Query and +0.8% Recall@1 accuracy in Image Query. With the spatial loss only, the model shows a consistent enhancement in performance compared to the baseline model, *i.e.*, +0.1% Recall@1 accuracy in Text Query and +0.1% Recall@1 accuracy in Image Query. With our method, the evaluation result shows a notable increase, *i.e.*, +0.5% Recall@1 in Text Query and +1.2% Recall@1 in Image Query. Therefore, the full model has arrived at the best performance with the two losses together, *i.e.*, 13.7% Recall@1 in Text Query and 26.2% Recall@1 in Image Query. We could observe that grounding loss is the main factor in enhancing retrieval performance. The combination of both losses could consistently perform better than only using one of them.

Different training sets. We study the effect of the dataset split in Table 5. The “satellite + Drone + Ground” training

Method	# Params	# Pre-train Images	GeoText-1652					
			Text Query			Image Query		
			R@1	R@5	R@10	R@1	R@5	R@10
UNITER [6]	300M	4M	0.9	2.7	4.2	2.5	7.4	11.8
METER-Swin [11]	380M	4M	1.3	3.9	5.8	2.7	8.0	12.2
ALBEF [17]	210M	4M	1.8	4.8	7.1	2.9	8.1	12.4
ALBEF [17]	210M	14M	1.1	3.5	5.3	3.0	9.1	14.2
XVLM [46]	216M	4M	4.3	9.1	13.2	4.9	14.2	21.1
XVLM [46]	216M	16M	4.5	9.9	13.4	5.0	14.4	21.4
UNITER _{finetuned}	300M	4M	10.6	20.4	26.1	21.4	43.4	59.5
METER-Swin _{finetuned}	380M	4M	11.3	21.5	27.3	22.7	46.3	60.7
ALBEF _{finetuned}	210M	4M	12.3	22.8	28.6	22.9	49.5	62.3
ALBEF _{finetuned}	210M	14M	12.5	22.8	28.5	23.2	49.7	62.4
XVLM _{finetuned}	216M	4M	13.1	23.5	29.2	23.6	50.0	63.2
XVLM _{finetuned}	216M	16M	13.2	23.7	29.6	25.0	52.3	65.1
Ours	217M	16M	13.7(+0.5)	25.7(+2.0)	32.3(+2.7)	26.2(+1.2)	53.5(+1.2)	66.4(+1.3)

Table 3. **Image-text bi-direction retrieval results on the GeoText-1652 dataset.** Text Query: Drone Navigation (Text-to-Image Search). Image Query: Drone-view Geo-localization (Image-to-Text Search). We show Recall@K with K = 1, 5, 10, as the evaluation metric.

Method	Text Query			Image Query		
	R@1	R@5	R@10	R@1	R@5	R@10
Baseline [46]	13.2	23.7	29.6	25.0	52.3	65.1
w grounding loss	13.5	25.4	31.7	25.8	53.0	65.9
w spatial loss	13.3	23.9	29.8	25.1	52.5	65.3
Ours	13.7	25.7	32.3	26.2	53.5	66.4

Table 4. **Ablation study results on different losses.** Baseline denotes that both spatial loss and bbox loss are ablated. We could observe that the full model could achieve the best retrieval performance in both test query and image query tasks.

Training Set	#imgs	Text Query			Image Query		
		R@1	R@5	R@10	R@1	R@5	R@10
Drone	37,854	13.1	23.6	29.4	25.4	51.3	63.2
Satellite + Ground	12,364	10.4	19.2	24.5	18.5	38.7	50.2
Satellite + Drone + Ground	50,218	13.7	25.7	32.3	26.2	53.5	66.4

Table 5. **Ablation study on different training sets.** The Recall@K are reported in percentage and higher is better. We could observe that using all images from three platforms could facilitate cross-modality matching.

λ	Text Query			Image Query		
	R@1	R@5	R@10	R@1	R@5	R@10
1.00	10.0	21.2	27.4	20.6	47.1	60.2
0.50	11.1	22.4	29.2	22.8	50.0	62.6
0.10	13.7	25.7	32.3	26.2	53.5	66.4
0.05	12.8	24.4	31.0	24.5	52.7	64.9

Table 6. **Ablation study on the hyper-parameter λ selection.**

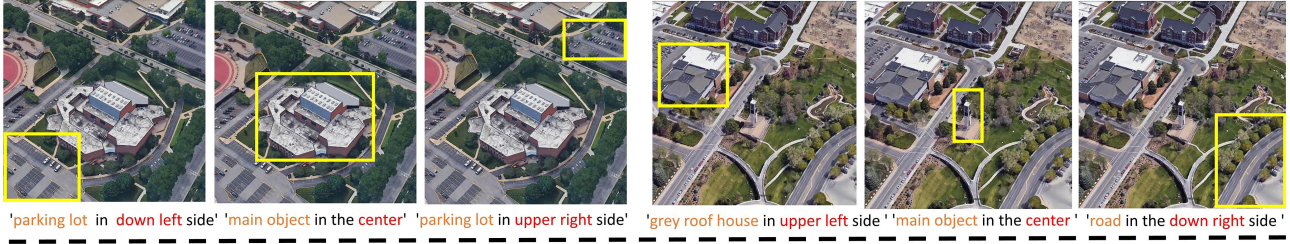
set shows its performance better than only using “Drone” or “Satellite + Ground” *i.e.* +0.6% Recall@1 in Text Query and +0.8% Recall@1 in Image Query compared to “Drone” training set, and +3.3% Recall@1 in Text Query and +7.7% Recall@1 in Image Query compared to “Satellite +

Ground” training set. These results indicate that when the training set includes a more diverse range of data (for instance, a combination of satellite, drone, and ground data), there is generally an improvement in performance across these tasks.

Hyperparameter Study. λ is the weight to balance the spatial matching losses and the image-text cross-modality matching losses. As shown in Table 6, we could observe that when $\lambda = 0.1$, the learned mode achieves the best recall accuracy.

Spatial Text Grounding. We further evaluate our spatial bounding box prediction on both synthesized and actual drone-view images (see Figure 5). It shows the strength in spatial matching, not just on familiar, trained images but also on new, real-world scenes. For instance, buildings and objects on the sea are never included in our training data, but the model could easily capture the boats and buildings based on our text instruction which indicates that the model has the potential to handle real-world navigation tasks. The images also accentuate the robustness in discerning between objects solely based on textual descriptions that define their spatial relationships, even when multiple instances of the same object are present within the same image. For example, when two parking lots are shown in the synthesized image, the model could detect the proposed parking lot just based on the spatial word we provided. Also, as shown in the real drone image, when a harbour with boats on both sides, the model could also capture the proposed object based on the instruction words. This level of fine-grained discrimination emphasizes the advanced understanding of spatial language, accurately mapping words that convey spatial relationships to the specific regions of the image they describe.

Spatial Bbox Prediction on Synthesized Drone View



Spatial Bbox Prediction on Real Drone View

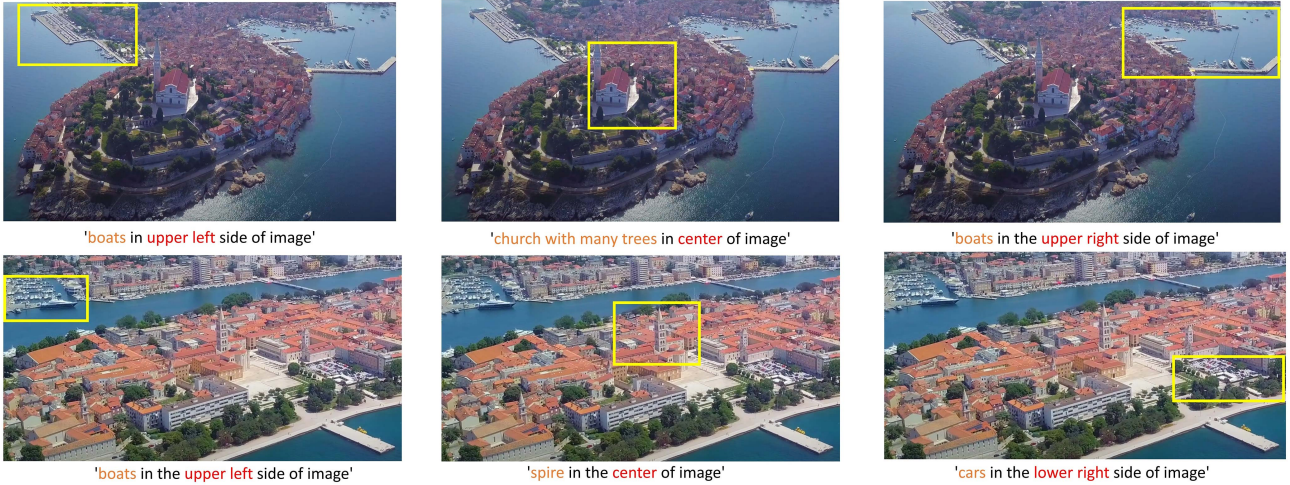


Figure 5. **Bounding box prediction on unseen images which includes images from our test set and the real drone view.** Our approach predicts correct regions even though there are so many same objects on the image which only have differences in spatial relationship textual descriptions differ in spatial relationship words. Our approach can also align each word in the text to the corresponding image region.

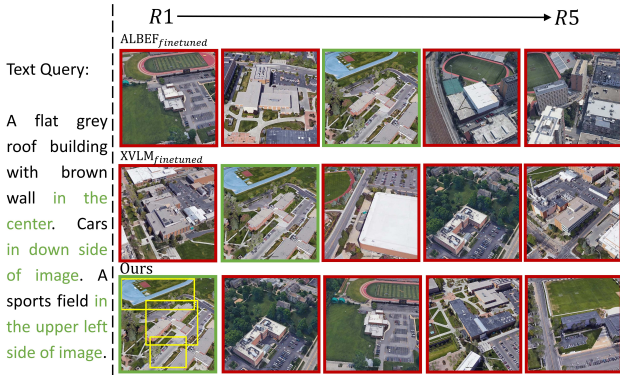


Figure 6. **Qualitative text-to-image retrieval results.** Between our method and baseline, placing in descending order from right to left based on similarity. The green boxes indicate the correct matches, and the images in the red boxes are the wrong matches. The green text highlights the details that our results match.

Text Query Retrieval. As shown in Figure 6, our method shows spatial-aware capabilities, achieving a higher recall compared to baseline models. When spatial descriptors are provided, our model effectively captures this information, enabling accurate image identification based not only on object labels but also on the integration of spatial relations. For

instance, the keywords, *e.g.*, “in the center”, “in the down side”, and “in upper left”, are well captured by our learned model. These keywords help the model to find the object of the target, which enhances the recall rate in the whole retrieval process. The results in the top rows show that the baseline still could retrieve the content-similar image, *e.g.*, a car, sports field or colour, but they miss the spatial alignment, which is common in real-world scenarios.

6. Conclusion

In this work, we introduce GeoText-1652, a new vision-language dataset that enhances natural language-guided drone navigation, addressing the challenges of dataset availability and alignment of language with fine-grained visual representations. The dataset enables two tasks: text-to-image and image-to-text retrieval for precise drone navigation and target localization. We also introduce a new blending spatial matching, leveraging region-level relationships between drone-view images and textual descriptions. The proposed method outperforms other cross-modality approaches in recall accuracy and shows good generalization in real-world scenarios.

References

- [1] Gabriele Berton, Riccardo Mereu, Gabriele Trivigno, Carlo Masone, Gabriela Csurka, Torsten Sattler, and Barbara Caputo. Deep visual geo-localization benchmark. In *CVPR*, pages 5396–5407, 2022. 2
- [2] Valts Blukis, Yannick Terme, Eyvind Niklasson, Ross A Knepper, and Yoav Artzi. Learning to map natural language instructions to physical quadcopter control using simulated flight. *arXiv:1910.09664*, 2019. 1
- [3] Shawn Brunsting, Hans De Sterck, Remco Dolman, and Teun van Sprundel. Geotexttagger: High-precision location tagging of textual documents using a natural language processing approach, 2016. 1
- [4] Meghan Chandarana, Erica L Meszaros, Anna Trujillo, and B Danette Allen. ‘fly like this’: Natural language interface for uav mission planning. In *International Conference on Advances in Computer-Human Interactions*, number NF1676L-26108 in NASA, 2017. 1
- [5] Guanlin Chen, Pengfei Zhu, Bing Cao, Xing Wang, and Qinghua Hu. Cross-drone transformer network for robust single object tracking. *IEEE Transactions on Circuits and Systems for Video Technology*, 2023. 2
- [6] Yen-Chun Chen, Linjie Li, Licheng Yu, Ahmed El Kholy, Faisal Ahmed, Zhe Gan, Yu Cheng, and Jingjing Liu. Uniter: Universal image-text representation learning. In *European conference on computer vision*, pages 104–120. Springer, 2020. 3, 7
- [7] Ming Dai, Jianhong Hu, Jiedong Zhuang, and Enhui Zheng. A transformer-based feature segmentation and region alignment method for uav-view geo-localization. *IEEE Transactions on Circuits and Systems for Video Technology*, 32(7): 4376–4389, 2021. 2
- [8] Jacob Devlin, Ming-Wei Chang, Kenton Lee, and Kristina Toutanova. Bert: Pre-training of deep bidirectional transformers for language understanding. *arXiv:1810.04805*, 2018. 6
- [9] Aayush Dhakal, Adeel Ahmad, Subash Khanal, Sriku-mar Sastry, and Nathan Jacobs. Sat2cap: Mapping fine-grained textual descriptions from satellite images. *arXiv:2307.15904*, 2023. 2
- [10] Carl Doersch, Abhinav Gupta, and Alexei A Efros. Unsupervised visual representation learning by context prediction. In *ICCV*, pages 1422–1430, 2015. 6
- [11] Zi-Yi Dou, Yichong Xu, Zhe Gan, Jianfeng Wang, Shuohang Wang, Lijuan Wang, Chenguang Zhu, Pengchuan Zhang, Lu Yuan, Nanyun Peng, et al. An empirical study of training end-to-end vision-and-language transformers. In *CVPR*, pages 18166–18176, 2022. 3, 7
- [12] Wenmiao Hu, Yichen Zhang, Yuxuan Liang, Yifang Yin, Andrei Georgescu, An Tran, Hannes Kruppa, See-Kiong Ng, and Roger Zimmermann. Beyond geo-localization: fine-grained orientation of street-view images by cross-view matching with satellite imagery. In *ACM MM*, pages 6155–6164, 2022. 2
- [13] Xuke Hu, Yingjie Hu, Bernd Resch, and Jens Kersten. Geographic information extraction from texts (geoext). In *European Conference on Information Retrieval*, pages 398–404. Springer, 2023. 1
- [14] Baichuan Huang, Deniz Bayazit, Daniel Ullman, Nakul Gopalan, and Stefanie Tellex. Flight, camera, action! using natural language and mixed reality to control a drone. In *2019 International Conference on Robotics and Automation (ICRA)*, pages 6949–6956. IEEE, 2019. 1
- [15] Chao Jia, Yinfei Yang, Ye Xia, Yi-Ting Chen, Zarana Parekh, Hieu Pham, Quoc Le, Yun-Hsuan Sung, Zhen Li, and Tom Duerig. Scaling up visual and vision-language representation learning with noisy text supervision. In *International conference on machine learning*, pages 4904–4916. PMLR, 2021. 1, 3
- [16] Hyo Jin Kim, Enrique Dunn, and Jan-Michael Frahm. Learned contextual feature reweighting for image geo-localization. In *CVPR*, pages 2136–2145, 2017. 2
- [17] Junnan Li, Ramprasaath Selvaraju, Akhilesh Gotmare, Shafiq Joty, Caiming Xiong, and Steven Chu Hong Hoi. Align before fuse: Vision and language representation learning with momentum distillation. *NeurIPS*, 34:9694–9705, 2021. 1, 2, 3, 7
- [18] Junnan Li, Dongxu Li, Caiming Xiong, and Steven Hoi. Blip: Bootstrapping language-image pre-training for unified vision-language understanding and generation. In *International Conference on Machine Learning*, pages 12888–12900. PMLR, 2022. 3
- [19] Kunpeng Li, Yulun Zhang, Kai Li, Yuanyuan Li, and Yun Fu. Visual semantic reasoning for image-text matching. In *ICCV*, pages 4654–4662, 2019. 3
- [20] Xiujuan Li, Xi Yin, Chunyuan Li, Pengchuan Zhang, Xiaowei Hu, Lei Zhang, Lijuan Wang, Houdong Hu, Li Dong, Furu Wei, et al. Oscar: Object-semantics aligned pre-training for vision-language tasks. In *Computer Vision—ECCV 2020: 16th European Conference, Glasgow, UK, August 23–28, 2020, Proceedings, Part XXX 16*, pages 121–137. Springer, 2020. 3
- [21] Jinliang Lin, Zhedong Zheng, Zhun Zhong, Zhiming Luo, Shaozi Li, Yi Yang, and Nicu Sebe. Joint representation learning and keypoint detection for cross-view geo-localization. *IEEE Transactions on Image Processing*, 31: 3780–3792, 2022. 2
- [22] Liu Liu and Hongdong Li. Lending orientation to neural networks for cross-view geo-localization. In *The IEEE Conference on Computer Vision and Pattern Recognition (CVPR)*, 2019. 4
- [23] Shilong Liu, Zhaoyang Zeng, Tianhe Ren, Feng Li, Hao Zhang, Jie Yang, Chunyuan Li, Jianwei Yang, Hang Su, Jun Zhu, et al. Grounding dino: Marrying dino with grounded pre-training for open-set object detection. *arXiv:2303.05499*, 2023. 4
- [24] Ze Liu, Yutong Lin, Yue Cao, Han Hu, Yixuan Wei, Zheng Zhang, Stephen Lin, and Baining Guo. Swin transformer: Hierarchical vision transformer using shifted windows. In *ICCV*, pages 10012–10022, 2021. 6
- [25] Ilya Loshchilov and Frank Hutter. Decoupled weight decay regularization. *arXiv:1711.05101*, 2017. 6

- [26] Jun-Ichi Meguro, Kiitirou Ishikawa, Takumi Hasizume, Jun-Ichi Takiguchi, Itsuki Noda, and Mitunori Hatayama. Disaster information collection into geographic information system using rescue robots. In *2006 IEEE/RSJ International Conference on Intelligent Robots and Systems*, pages 3514–3520. IEEE, 2006. **1**
- [27] Abolfazl Mehdodniya, Julian L Webber, Sathishkumar Karupusamy, et al. Improving the geo-drone-based route for effective communication and connection stability improvement in the emergency area ad-hoc network. *Sustainable Energy Technologies and Assessments*, 53:102558, 2022. **1**
- [28] OpenAI. Gpt-4 technical report, 2023. **4**
- [29] Alec Radford, Jong Wook Kim, Chris Hallacy, Aditya Ramesh, Gabriel Goh, Sandhini Agarwal, Girish Sastry, Amanda Askell, Pamela Mishkin, Jack Clark, et al. Learning transferable visual models from natural language supervision. In *International conference on machine learning*, pages 8748–8763. PMLR, 2021. **1, 3**
- [30] Md Tahmid Rashid, Daniel Yue Zhang, and Dong Wang. Socialdrone: An integrated social media and drone sensing system for reliable disaster response. In *IEEE INFOCOM 2020 - IEEE Conference on Computer Communications*, pages 218–227, 2020. **1**
- [31] Hamid Rezaatofighi, Nathan Tsoi, JunYoung Gwak, Amir Sadeghian, Ian Reid, and Silvio Savarese. Generalized intersection over union: A metric and a loss for bounding box regression. In *CVPR*, pages 658–666, 2019. **5**
- [32] Royston Rodrigues and Masahiro Tani. Are these from the same place? seeing the unseen in cross-view image geo-localization. In *WACV*, pages 3753–3761, 2021. **1**
- [33] Royston Rodrigues and Masahiro Tani. Global assists local: Effective aerial representations for field of view constrained image geo-localization. In *WACV*, pages 3871–3879, 2022. **2**
- [34] Yujiao Shi and Hongdong Li. Beyond cross-view image retrieval: Highly accurate vehicle localization using satellite image. In *CVPR*, pages 17010–17020, 2022. **2**
- [35] Yujiao Shi, Liu Liu, Xin Yu, and Hongdong Li. Spatial-aware feature aggregation for image based cross-view geo-localization. *NeurIPS*, 32, 2019. **1**
- [36] Bo Sun, Ganchao Liu, and Yuan Yuan. F3-net: Multi-view scene matching for drone-based geo-localization. *IEEE Transactions on Geoscience and Remote Sensing*, 61:1–11, 2023. **1**
- [37] Gabriele Trivigno, Gabriele Berton, Juan Aragon, Barbara Caputo, and Carlo Masone. Divide&classify: Fine-grained classification for city-wide visual geo-localization. In *ICCV*, pages 11142–11152, 2023. **2**
- [38] Ashish Vaswani, Noam Shazeer, Niki Parmar, Jakob Uszkoreit, Llion Jones, Aidan N Gomez, Łukasz Kaiser, and Illia Polosukhin. Attention is all you need. *NeurIPS*, 30, 2017. **4**
- [39] Kunyu Wang, Xueyang Fu, Yukun Huang, Chengzhi Cao, Gege Shi, and Zheng-Jun Zha. Generalized uav object detection via frequency domain disentanglement. In *CVPR*, pages 1064–1073, 2023. **2**
- [40] Tingyu Wang, Zhedong Zheng, Chenggang Yan, Jiyong Zhang, Yaoqi Sun, Bolun Zheng, and Yi Yang. Each part matters: Local patterns facilitate cross-view geo-localization. *IEEE Transactions on Circuits and Systems for Video Technology*, 32(2):867–879, 2021. **2**
- [41] Zihao Wang, Xihui Liu, Hongsheng Li, Lu Sheng, Junjie Yan, Xiaogang Wang, and Jing Shao. Camp: Cross-modal adaptive message passing for text-image retrieval. In *ICCV*, pages 5764–5773, 2019. **3**
- [42] Scott Workman, Richard Souvenir, and Nathan Jacobs. Wide-area image geolocation with aerial reference imagery. In *IEEE International Conference on Computer Vision (ICCV)*, pages 1–9, 2015. Acceptance rate: 30.3%. **4**
- [43] Hongji Yang, Xiufan Lu, and Yingying Zhu. Cross-view geo-localization with layer-to-layer transformer. *NeurIPS*, 34:29009–29020, 2021. **2**
- [44] Shuyu Yang, Yinan Zhou, Zhedong Zheng, Yaxiong Wang, Li Zhu, and Yujiao Wu. Towards unified text-based person retrieval: A large-scale multi-attribute and language search benchmark. In *ACM MM*, pages 4492–4501, 2023. **3**
- [45] Qian Yu, Chaofeng Wang, Barbaros Cetiner, Stella X Yu, Frank Mckenna, Ertugrul Taciroglu, and Kincho H Law. Building information modeling and classification by visual learning at a city scale. *arXiv:1910.06391*, 2019. **1**
- [46] Yan Zeng, Xinsong Zhang, and Hang Li. Multi-grained vision language pre-training: Aligning texts with visual concepts, 2022. **2, 3, 6, 7**
- [47] Qi Zhang, Zhen Lei, Zhaoxiang Zhang, and Stan Z Li. Context-aware attention network for image-text retrieval. In *CVPR*, pages 3536–3545, 2020. **1**
- [48] Xiaohan Zhang, Xingyu Li, Waqas Sultani, Yi Zhou, and Safwan Wshah. Cross-view geo-localization via learning disentangled geometric layout correspondence. In *AAAI*, pages 3480–3488, 2023. **1, 2**
- [49] Zhedong Zheng, Yunchao Wei, and Yi Yang. University-1652: A multi-view multi-source benchmark for drone-based geo-localization. In *ACM MM*, pages 1395–1403, 2020. **1, 2**
- [50] Zhedong Zheng, Liang Zheng, Michael Garrett, Yi Yang, Mingliang Xu, and Yi-Dong Shen. Dual-path convolutional image-text embeddings with instance loss. *ACM Transactions on Multimedia Computing, Communications, and Applications (TOMM)*, 16(2):1–23, 2020. **3**
- [51] Deyao Zhu, Jun Chen, Xiaoqian Shen, Xiang Li, and Mohamed Elhoseiny. Minigt-4: Enhancing vision-language understanding with advanced large language models. *arXiv:2304.10592*, 2023. **4**
- [52] Pengfei Zhu, Longyin Wen, Dawei Du, Xiao Bian, Heng Fan, Qinghua Hu, and Haibin Ling. Detection and tracking meet drones challenge. *IEEE Transactions on Pattern Analysis and Machine Intelligence*, 44(11):7380–7399, 2021. **1**
- [53] Sijie Zhu, Taojiannan Yang, and Chen Chen. Vigor: Cross-view image geo-localization beyond one-to-one retrieval. In *CVPR*, pages 3640–3649, 2021. **4**
- [54] Sijie Zhu, Mubarak Shah, and Chen Chen. Transgeo: Transformer is all you need for cross-view image geo-localization. In *CVPR*, pages 1162–1171, 2022. **2**